Tribological and Corrosion Behavior of AISI 1045 Coated with AISI 316 Film Produced By Triode Magnetron Sputtering

Silviane C. F. Gorski[a]* ⓘ *, Bruno Nunes[a]* ⓘ *, Abel A. C. Recco[a]* ⓘ *, Cesar E. da Costa[a],*

Marcus V. F. Schroeder[a], Julio C. Giubilei Milan[a] ⓘ

[a] Universidade do Estado de Santa Catarina, Programa de Pós-graduação em Ciências e Engenharia de Materiais, Rua Paulo Malschitzki, 200, 89.219-710, Joinville, SC, Brasil.

Recent studies have demonstrated mechanical, tribological and corrosion improvements properties on raw materials coated with stainless steel films produced by magnetron sputtering. However, few studies have reported the tribological behavior of thin austenitic stainless-steel films applied to the surface of carbon steels. The present study investigated the tribological behavior of AISI 1045 carbon steel coated with AISI 316 stainless steel film. Pin-on-disc dry sliding wear test was performed. The wear tracks were analyzed using a scanning electron and confocal microscopes. The corrosion resistance of coated and uncoated AISI 1045 were also assessed through an electrochemical test. Samples which presented a mixture of α-Ferrite and γ-iron, with predominant austenite parts, demonstrated lower friction coefficient, lower wear rates, and better corrosion resistance compared to substrate material. The results were also influenced by the variables used in the deposition process, as observed, heating the substrate and submitting to a higher powder density could improve the results. The results found corroborate to the academic and industrial research which looks for coating alternatives to AISI 1045 tools.

Keywords: *Sliding Wear, Thin films, Magnetron Sputtering, Corrosion Resistance, Triode Magnetron Sputtering, Stainless Steel Films.*

1. Introduction

AISI 1045 carbon steel is widely used to produce tools and molds. AISI 1045 is known for its good machinability, weldability, and mechanical impact resistance. It is a steel with few alloying elements, normally has low corrosion resistance compared to stainless steel, which compromises the useful life of molds and tools produced with AISI 1045[1].

Stainless steel has better corrosion resistance compared to conventional carbon steel, therefore films obtained from sputtering austenitic stainless steel (ASS) targets become an alternative to improve mechanical and corrosion properties of AISI 1045. Yoo et al.[2] investigated the carbon steel coated with AISI 304 stainless steel (ASS) film produced by unbalanced magnetron sputtering. The results were considered acceptable for the mechanical properties and corrosion resistance of the coated samples compared to the substrate material. España Peña et al.[3] studied the AISI 316 coating obtained by TMS applied on a similar chemical composition sample of the target, AISI 316 austenitic substrate, results demonstrated higher hardness on coated AISI 316[3]. Around 20 years ago, magnetron sputtering techniques (MS) and their variations to produce thin films have been investigated[4], but there are few studies about specific parts coated with stainless steel films produced by unbalanced magnetron configuration or Triode Magnetron Sputtering technique (TMS)[5]. The benefits

of the TMS technique have been evidenced in some works referenced[5-11].

Researchers[9-16] have reported that the changes in the coated materials properties are associated to the structural changes of AISI 316 film deposited on substrate materials. Magnetron sputtering, pulsed, or non-pulsed discharge coating processes modifies the crystalline structure, consequently the grain size. The crystalline changes of layers formed have been related to reduction in the defects, consequently it influences not only roughness but also microhardness and thickness of the substrate[12-14,16].

This structural change provides an increase in strength, and this increase is suggested to occur on both substrate material types, forged and cold work shaped. Materials substrate structures, for example, carbon steel has preferential ferrite phase (BCC), after the coating process when AISI 316 film is deposited, the coated sample presents parts of BCC iron (α-Ferrite) and FCC austenite (γ-iron)[9-15]. According to parameters differences of coatings produced by TMS, the carbon steel coated presented preferential austenite (FCC) structure, and the stainless steel coated with stainless steel target presented only ferrite (BCC) structure, results observed through X-ray diffraction analysis (XRD) and reported by Schroeder et al.[11]. Studies to obtain stainless steel films, as well as the technique to be used, the benefits in terms of adhesion quality and properties improvement, including thermodynamics details between de BCC and FCC structures

are easily found in the literature[11,15]. Nonetheless, a few studies about tribological and corrosion investigation of carbon steels coated with AISI 316 are found[2,9-11].

Therefore, the present article aims to analyze the tribological behavior of AISI 1045 coated with AISI 316, and to evaluate the effects of electrochemical corrosion test on coated and uncoated material.

2. Materials and Methods

AISI 1045 carbon steel was used as substrate. Substrate was coated in laboratory experiments. AISI 1045 substrate and AISI 316 target chemical compositions are described in Table 1.

Production details of the coating, about the equipment, and its commercial apparatus used, including the configuration of the triode magnetron sputtering system (TMS), used to coat the samples used in this work are available in details in Fontana and Muzart[5-7], Schroeder[9] and Schroeder et al.[11]. Table 2 shows the parameters of power density, sample temperature, and pulse for the deposition of AISI 316 film, as observed, there is a different deposition condition for each sample, enabling the production of different coatings structures.

Table 3 describes the crystalline structures proportions of the coating conditions detailed in Table 2. These data were extracted from the study carried out by Schroeder[9] to assist the discussion about wear and corrosion results of the present study.

2.1. Friction coefficient and wear experimental details

Six samples were submitted to pin-on-disc sliding wear test to evaluate the coefficient of friction (COF) and the wear rate (WR). The sliding wear test run at room temperature, dry condition (without lubrication), and relative humidity at approximately 70%, as suggested in Standard Test Method for Wear Testing with a Pin-on-Disc apparatus (ASTM G99-05 reapproved 2010). As the number of samples was limited, a variation in the track radius was performed, the same conditions (different track radius) were reproduced to every sample. Four tracks of each sample were analyzed. The variables (speed, load, and distance) were fixed for all samples. The speed applied was 0.05 m/s, at a load of 2 N for 50 m distance. The counter-body used was a 6 mm diameter alumina (Al_2O_3) sphere. The parameters used during the wear tests are described in Table 4 and Figure 1 shows a schematic illustration of the pin-on-disc equipment used.

Confocal microscopy was used to analyze the wear tracks produced during the pin-on-disc test. Four regions were mapped in each track, then the average wear profile was obtained, as observed in Figure 2.

Figure 2 shows the illustration of a mapped region of the wear tracks. Figure 2a represents the positions where the images were acquired, the three-dimensional topographic image of the wear track is illustrated in Figure 2b. Figure 2c shows the area where multiple profiles are acquired in order to obtain an average profile shown in Figure 2d, which enables

Table 1. Chemical compositions (wt.%)[11].

Material	C	Cr	Ni	Mn	Mo	Fe
AISI 316 target	0.03	17.0	9.5	1.8	2.1	Balance
AISI 1045 substrate	0.45	0.0	0.0	0.8	0.0	Balance

Table 2. TMS deposition settings[11].

Conditions	Power density (W.cm^{-2})	Samples Temperature (K)	Pulse frequencies (kHz)
C1	3.08	Not heated	Non-pulsed (DC)
C2	7.26	Not heated	Non-pulsed (DC)
C3	11.3	Not heated	Non-pulsed (DC)
C4	15.8	Not heated	Non-pulsed (DC)
C5	15.8	673 K	Non-pulsed (DC)
C6	15.8	673 K	150

Table 3. Crystalline structures, thickness values and phase proportions of the samples coated with ASS film[9-11].

Conditions	Thickness (μm)	Crystalline structures and phase proportions (%)	
C1/R1*	1.3±0.03	BCC (α-Ferrite)	100%
C2	2.1±0.05	BCC (α-Ferrite)	100%
C3	4.4±0.10	BCC (α-Ferrite)	100%
C4	4.0±0.08	BCC (α-Ferrite)	100%
C5	1.4±0.01	BCC (α-Ferrite) +	56%+44%
R3*		FCC (γ-austenite)	45%+55%
C6	2.9±0.15	BCC (α-Ferrite) +	4%+87%
R2*		FCC (γ-austenite)	19%+81%

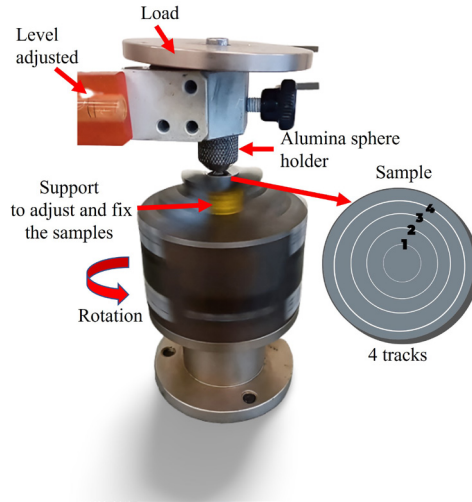* R1, R2, and R3 were used for polarization corrosion test.

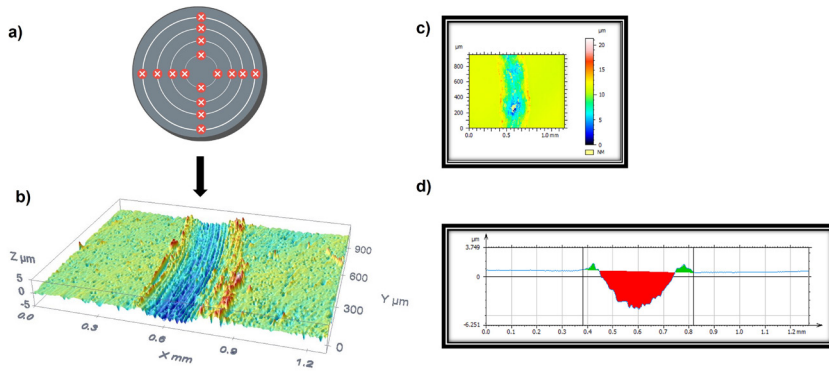**Figure 1.** Pin-on-disc schematic and the illustration of sample wear tracks.

Figure 2. a) Illustration of the 4 mapping regions in each worn track, b) Worn track image obtained by confocal microscopy software analysis, c) Three-dimensional graphs of a surface mapped, and d) Average profile extracted from three-dimensional graphs, showing between the highlighted bars the area required for wear volume determination.

Table 4. Pin-on-disc wear sliding test conditions.

Samples	AISI 1045 and Coated samples
Sliding distance	50 m
Load applied	2 N
Sliding speed	0.05 m/s
Counter-body	Polished alumina ball (Al_2O_3), θ=6.0 mm

the determination of the worn area highlighted between the bars. The coefficient of friction (μ) was measured through the friction force (F_x) obtained during pin-on-disc test and divided by normal force (F_z) applied. The calculations were expressed by $\mu = F_x / F_z$. The steady state average of the coefficient of friction (μ) was plotted in Figure 3 (section 3). The volume of material removed (*VMR*), in mm³, was according to the ASTM G99 standard and tested by Blau[17] as shown in Equation 1. Where the total wear area ($A_{wear\ track}$)

is the difference between the valley (A_{valley}) and peak (A_{peak}) areas, in mm², and r is the radius of the tracks.

$$VMR = 2\pi r_{wear\ track} \ x \ A_{wear\ track} \qquad (1)$$

The results of volume of material removed (VMR) obtained were used to calculate the wear rate (WR), in mm³/N.m, according to Equation 2 described by Archard and Hirts[18]. Where, C is the normal load, in N, and D is the total sliding wear distance, in m.

$$WR = \frac{VMR}{CxD} \qquad (2)$$

2.2. Corrosion resistance experimental details

The corrosion resistance of coated and uncoated AISI 1045 were evaluated through an electrochemical test. Three samples selected are represented by R1, R2 and R3. These

samples used in the corrosion test had similar crystalline structures compared to the samples that were submitted to the wear test. Samples comparisons are presented in Table 3. The equipment used was a Gamry potentiostat, model IFC1010-28233. The equipment has an acquisition limit from 10 nA to 100 mA. Three electrodes were used, Platinum counter electrode, cell's reference electrode as Ag|AgCl, and the working electrode or sense as the sample. Before starting the potentiodynamic polarization test, 1 cm² of the surface of each sample was analyzed in an immersion saline solution (3.5% NaCl by weight) with an open circuit (OCP) for 3 hours to stabilize the system. First the OCP test was performed above +400 mV on the anode side, with a scan rate of 1mV/s. After the OCP test, the potentiodynamic polarization test is automatically started, where the cathodic potential starts at -1000 mV until reaches the anode potential at +600 mV, with an acquisition rate of 1 mA/cm². Parameters were defined according to the literature[2,19].
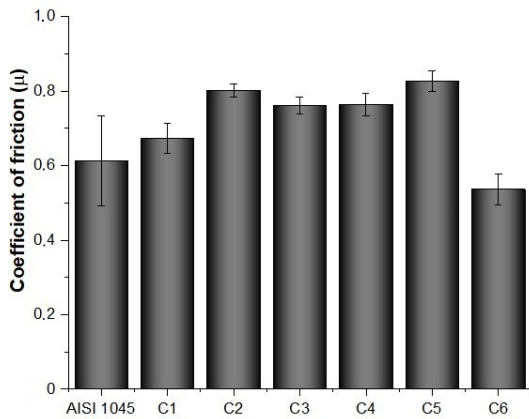
In addition to the characterization tests, scanning electron microscopy (SEM) and Energy dispersive X-ray spectroscopy (EDX) techniques were used.

3. Results and Discussion

3.1. Coefficient of friction – COF

Figure 3 shows the average coefficient of friction calculated for each experimental condition, considering the steady state of the tribological system.

In Figure 3, C6 condition presented the lower COF average among all the experimental conditions. Comparing AISI 1045 and C6 condition, COF decreased from 0.61 to 0.54 respectively, about 11% reduction of the friction coefficient when the material is coated. Comparing C6 sample to all other coated samples (C1 to C5), the average COF of C6 was lower reaching up to 30% reduction. A graphical analysis of the dynamic coefficient values allows better visualization of COF behavior for the samples considering 50 m test distance.

The COF curves can be seen in Figure 4. Figure 4a shows the dynamic COF behavior of conditions C6, C5, C4, and Figure 4b shows the dynamic COF behavior of C3, C2, and C1. The first graph, in both Figure 4a, b represents the behavior of uncoated AISI 1045 in order to make comparisons.

The red line drawn in Figure 4a, b separate two different regions. The first region is known as the transient state (Stage 1). The second region (Stage 2) is known as steady state[20]. The COF graphs for the coated samples presented irregular behavior in the first contacts between the counter-body and the samples surfaces, until it reaches Stage 2 (steady state) at about 15 m. Analyzing the COF behavior for the major conditions at Stage 1, it possible to affirm that the film breaks progressively. A few differences can be observed in C6 and C5, where regions 1 and 2 were
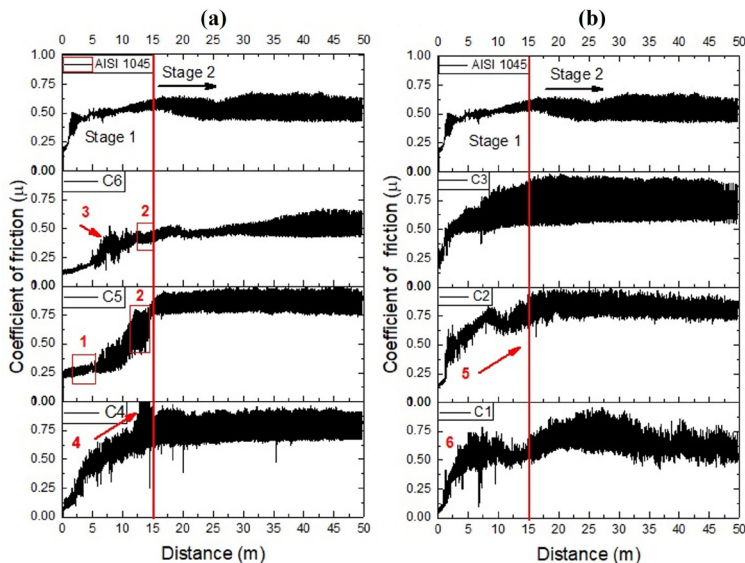

Figure 3. Coefficient of friction average.

Figure 4. (a) Coefficient of friction profile obtained to coated and uncoated AISI 1045 in the conditions C6, C5, C4, and (b) Coefficient of friction profile obtained to the uncoated AISI 1045, and to the coated conditions C3, C2, and C1.

highlighted. In general, at Stage 2 the COF fluctuation values were stabilized with some scattering.

The highlighted regions 3, 4, and 6 (Figure 4a, b) suggest that the oscillation of the COF values is related to the debris detached from the coated material. Considering the COF behavior of C5, in the highlighted region 1 (between 3 and 5 m of distance) some stability is noted. In sequence, another oscillation is observed through a friction coefficient increase, then the COF in region 2 (between 13 and 15 m of distance), seems to be a stable region. Two stable regions were observed for sample C5. Region 2 is also noted for the C6 coated sample but at a shorter distance. On the other hand, considering the conditions C3, C4, and AISI 1045, a fluctuation and a COF value increase were observed at Stage 1, and the highlighted region 4 suggests film delamination. In the highlighted regions 5 (C2), and 6 (C1) high fluctuations were detected. After 15 m sliding, the COF values of all conditions had reached a steady-state regimen, resulting in a stable tribosystem (Stage 2).

Narrowing to Stage 1, considering the first 10±5 m of sliding distance, it is relevant to state a reduction in the friction coefficient of the coated samples, C4, C5, and C6, comparing to AISI 1045. Conditions C5 and C6 conditions, at around 5±2 m of distance presented COF below 0.3. A similar result was found in España Peña et al.[3] study, in which they analyzed the tribological behavior of the AISI 316 thin film deposited on AISI 316 raw material, through a dry pin-on-disc test using an alumina ball counter-body, at a load of 1N and a sliding speed of 0.01m/s for 10 minutes. The authors reported a COF reduction from 0.7 to 0.5 when the samples were coated in an inert MS atmosphere, and a COF reduction from 0.7 to 0.35 for coatings obtained in a reactive MS atmosphere. Comparing the present work to the work of España Peña et al.[3], considering the first 10 min of sliding test (during stage 1), we can state the results were similar, pointing to a COF reduction to the coated samples. España Peña et al.[3,21] observed in their studies pile-up and semicircular crack failure at the edges of worn after scratch. The crack damage was considered a type of ductile tensile failure due to cracks damage in the direction of the scratch. Consequently, when the load increased, the density of the buckling cracks also increased. The authors also observed part of the wear material (debris) dragged by the indenter and located on the sides of the track. The fluctuation of friction observed can be attributed to the presence of debris which were removed or dragged in the worn track. This phenomenon explains the friction oscillation illustrated in Figure 4 (mainly at Stage 1).

Stachowiak and Batchelor[20] reported friction behavior as complex due to all processes of contact which could be involved as asperities, thermal effect, elastic relaxation resulting of film rupture until substrate is reached. Therefore, in dry contact, with high speed, where severe contact through two-body and three-body slip abrasion of the asperities or debris occur, causes wear and high friction[20]. In order to achieve a better comprehension of the COF complex fluctuations of the samples observed in Figure 4, results were analyzed and discussed as suggested by Godfrey[22], thus considering all values of dynamic friction coefficient, enabling the behavior analysis of surfaces in contact and friction during the sliding

wear test. During the sliding wear test, several COF fluctuations were observed and can be explained by the effects known as stick-slip observed in Zappelino et al.[23] studies. Stick-slip affects the COF stability because debris performs as solid lubricant resulting in a decrease and increase of COF values speedily at different times and distances of sliding wear test. Holmberg et al.[24] reported some experimental results of stainless-steel diamond coated against alumina counter-body after a dry sliding test, a decreased in wear and an increase in friction were observed. The COF values were reported in a range of 0.3-0.9[3,23,24]. Therefore, the COF value range shown in this research was expected to thin films coated in bare metals after dry sliding conditions[20-25].

According to Schroeder[9], Sa and Sq roughness observed through AFM microscope, results in variations between 1.0 nm and 7.8 nm. The coating roughness variations can be associated to the high impact of the magnetron sputtering atmospheres in different systems and due to the types of phases formed when compared to each other. The variation for the roughness between C5 and C6 (BCC+FCC) was around 0.7 nm, resulting in lower variation compared to other coated samples. In contrast comparing C1 and C4 (both BCC) the variation in roughness was about 4.9 nm. Therefore, there is a large variation in average roughness results among the BCC phase formed in different MS conditions. This could be related to higher friction fluctuations of these coated samples. The lower friction results observed, mainly at the beginning until 15 m of distance, were obtained to the samples with the lowest roughness average. Pointing better results for C5 and C6 conditions.

Some authors[23-28] have related the increased Sa and Sq value parameters to a lower friction coefficient when the steady regime is reached, considering a dry sliding contact system wear test for long distances. The application for high loads and long distances is not acceptable for ASS films due to the conditions selected for some studies[3,21,27]. This could be related because there are no diffusion processes. Despite that, the Sa and Sq results and friction performance follow similar results with other coatings in different sliding contact systems.

Garzón et al.[27] results presented a lower roughness (Sa) for samples coated with ASS in presence of ferrite phase (BCC) in comparison to nitrided samples. The authors also highlighted poor results of ASS coating produced by sputtering in a non-inert atmosphere and non-heated substrate.

Among all samples, condition C6 had a lower coefficient of friction result. The lowest COF values of coated AISI 1045 revealed a mixture of crystalline structure and phases: parts of BCC (ferrite-α), FCC (austenite-γ) with a higher percentage of FCC (austenite-γ). Few authors have reported that a significant COF decrease was observed in coated samples where FCC structure is predominant[3,4,21]. This mixture of structures and phases is also identified in C5.

3.2. Sliding wear behavior

The wear tracks were observed through SEM, enabling the observation and analysis of the wear mechanisms involved. The wear track formed after the sliding wear test is shown in Figure 5.

The wear tracks of C4 and C5 conditions are delimited by the arrows in Figure 5. It is observed that C4 presented a wider track width comparing to C5 track, pointing that C5 presented lower wear than C4. Considering that the worn track edges undergo less contact pressure between coated surfaces and counter-body[23], it is important to evaluate the depth reached in the profile in order to corroborate the results of volume of removed material, consequently, for wear rate results.

The red highlighted region signs were observed in all coated conditions, considering similarities between samples coated by the deposition carried out with substrate heating at 673 K (C5-C6), in contrast with these depositions carried without substrate heating (C1-C4).

In order to better represent this wear behavior evidence[23,28]. Figure 6 shows the representation of the medium profile highlighting the maximum depth reached in the removed material area of C4 (representing BCC and non-heated substrate in magnetron sputtering, Tables 2 and 3 for details) and C5 (representing BCC+FCC and heated substrate in magnetron sputtering, Table 2-3 for details).

The higher and lower thickness values among BCC films were respectively, 4.4 µm for C3 and 1.3 µm for C1 coated sample. And among BCC+FCC film the higher and lower thickness value was respectively, 2.9 µm for C6 and 1.4 µm for C5 coated sample (details in Table 3).

The average results of maximum depth reached to C1-C4 and C5-C6 conditions were 5.7±1.5 µm and 1.8±0.6 µm, respectively. Furthermore, the values of maximum depth can be correlated to the thickness values enabling identify the wear in proportion (%). The measurements are shown in Table 5[29].

Despite the wear severe observed. Through these results shown in Table 5, is possible to state that coated samples produced by magnetron sputtering with heated substrate and

Table 5. The maximum depth and thickness ratios (%), for conditions C1, C2, C4, C5, and C6 (after sliding wear test).

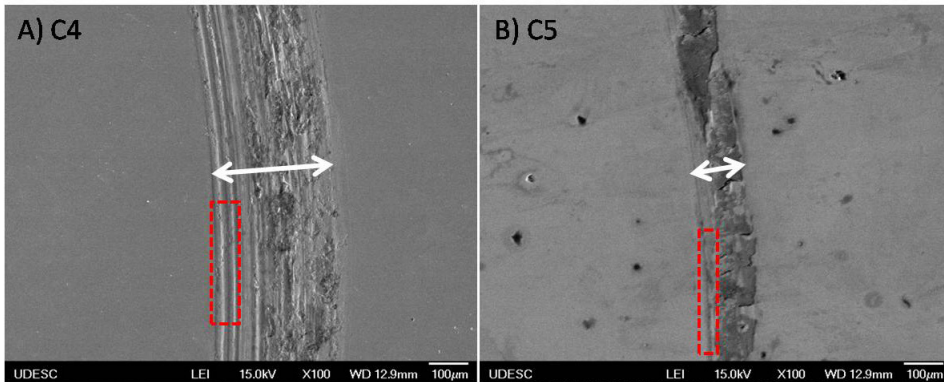| Conditions	Maximum Depth (µm)	Depth/Thickness (%)
C1	4.6 ± 1,5	353%
C2	4.5 ± 1,3	214%
C4	5.7 ± 1,6	142%
C5	0.9 ± 0.9	63%
C6	1.8 ± 0.6	63%

Figure 5. Micrographs of the wear tracks obtained of C4 and C5 coated conditions, after the pin-on-disc wear test.
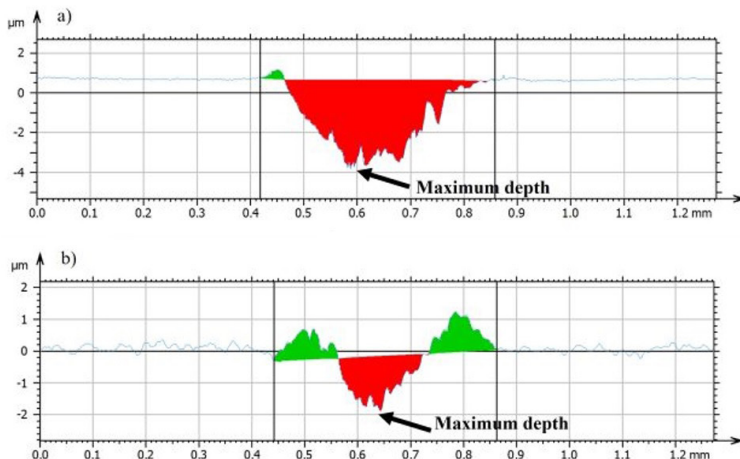

Figure 6. Profile of removed material area highlighting the maximum depth reached of coated AISI 1045 (a) C4 and (b) C5.

coatings that BCC+FCC phases were formed, presented, between 2 to 6 times, lowest wear than BCC configurations.

According to Shoreder[9,11] all coated samples (C1-C6 conditions) presented elastic modulus results varying between 194 and 218 GPa and hardness varying between 8.6 and 12.1 GPa. The lower hardness of 8.6±0.4 with elastic modulus of 195±12 GPa was evidenced for C1 condition. In contrast, the higher hardness of 12.1±0.7 with elastic modulus of 199±11 GPa was evidenced for C5 condition.

The differences in values of elastic modulus and hardness for all samples do not suggest a direct impact on tribological results. Nonetheless, the elastic modulus could be considered an important influence parameter for the toughness of the coating, consequently impacting wear results.
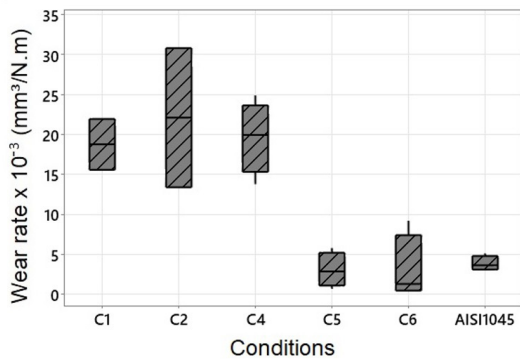

Figure 7. Wear rate values of uncoated AISI 1045 and coated in C1, C2, C4, C5, and C6 conditions.

The wear rate was calculated using a relationship between Equations 1 and 2 (see details in section 2), results are shown in Figure 7.

As shown in Figure 7, the wear rate reduction was a tendency to be significant for conditions C5 and C6. Applying ANOVA statistical test (significance level of α=0.05), the variances of all conditions are not so different, although a tendency to lower wear rate results due the reduction of the median point revealed for C5 and C6 conditions are observed in boxes, mainly for C6 condition. The wear test promoted total delamination of the coating from C3 condition impairing its analysis at the confocal microscope. C3 condition presented the higher coating thickness, which resulted in total delamination after the critical dry sliding wear test. On the other hand, Garzón et al.[27] studied SS coated by MS (with N_2 and inert flux flow), where film thickness varied between 3 and 5 μm. In their studies they applied indentation tests which can be considered less critical than dry sliding wear test. Their results showed that the coated samples produced by MS at 573 K (substrate heating) presented no crack formation up to 2 kgf Vickers indentation. Cracks occurred after 10 kgf Vickers indentation.

SEM Micrographs were obtained to enable the identification of the wear mechanisms and tribological behavior. Figure 8 shows the micrographs highlighting the worn tracks formed for C4 and C5 coated conditions in detail.

Figure 8a shows the region selected to perform detailed analysis which is seen in Figure 8b in a higher magnification. The wear rate increase can be explained and related to some factors observed during the wear tests. The sliding speed results in friction heat. The temperature increases proportionally
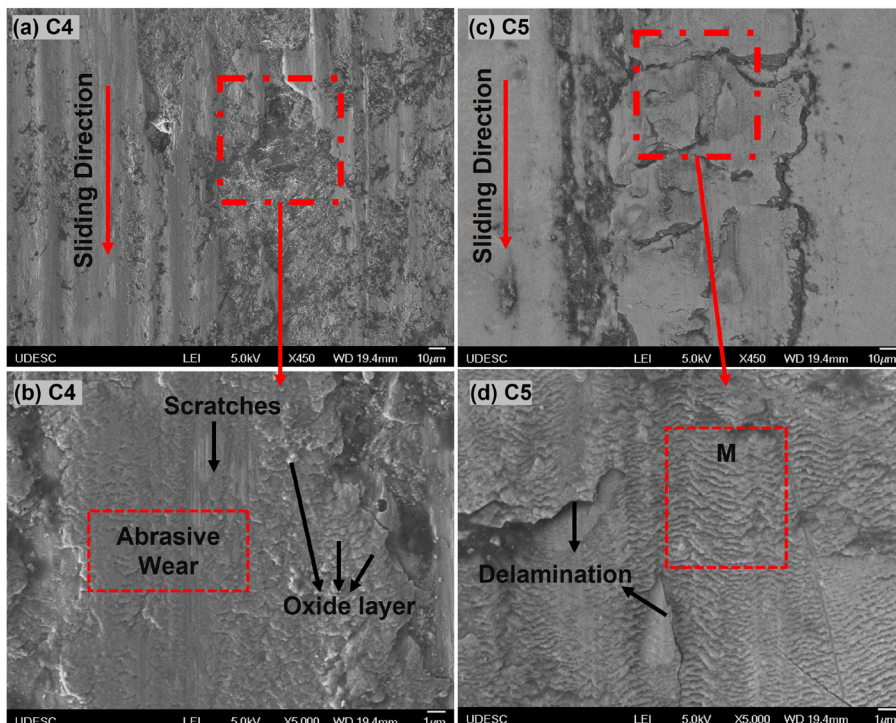

Figure 8. SEM images of the wear track of coated AISI 1045 (a) C4, (b) C4 in details, (c) C5, and (d) C5 in details.

to the increase in speed, consequently causing oxidation or oxide layer formation[24]. The oxide layer was identified in Figure 8b. The oxide layer mechanically formed during the sliding wear test suggests the indication of oxidative wear mechanisms but also abrasive wear[24,25].

In general, austenitic stainless-steel film (ASS) coating in both, forged or cold worked materials have been related to abrasive wear due to a higher concentration of stress or pressure of the tribo-pair in the tribological system, consequently increasing temperature in the friction area contributing to the oxide layer formation after dry sliding wear test[3]. In addition to oxygen, nickel can also be related to abrasive wear, due to a tenacious surface oxide layer which can be formed when a high Ni concentration is observed as found in the ASS composition. The oxidative wear mainly in dry sliding conditions can reduce wear and friction. In Figure 8b scratches were observed indicating signs of abrasive wear mechanism. All the facts mentioned have been correlated to abrasive wear mechanisms[20,25]. EDS analysis reveals the presence of elements such as oxygen, nickel, and others in the wt.% (Figure 8 and Table 6 of EDS analysis).

Figure 8c shows a selected region and in (d) the region can be observed in a higher magnification. Asperities can be observed in the surface of this region as illustrated in (d) they can be related to machining grooves reported by Stachowiak and Batchelor[20] due to their perpendicular sliding direction. According to Menezes et al.[25] the friction increases during the sliding wear test until it reaches a steady state. And then, in the steady state (see Stage 2, Figure 4), the

surface is subjected to plastic deformation. Therefore, due to plastic deformation highlighted in region M, the surface appearance can be compared to cracklike elongated voids. The ploughing term or grooving effect, when the material is pushed up and aside, is also very similar to the surface appearance in region M illustrated and it can be seen in other regions in Figure 8b-d. The ploughing plastic deformation effects can be better observed in Figure 9. In addition, the major cracks have been considered and observed in a perpendicular sliding direction[20,25].

Besides plastic deformation and debris spalling, the delamination mechanism also can be observed in Figure 8d[26]. Complementing the analysis in region M, Figure 9 shows the inner track in a higher magnification and indicates the different points where EDS analysis was held to quantify the present chemical elements.

The elements such as O, Ni, and Cr detected in Figure 9 confirmed signs of abrasive wear with ploughing and oxidative wear[22-26].

Figure 10 illustrates the region (a) worn track of C4 coated highlighting points Pt.1, on the edge and Pt.2 within the track. And the region (b) worn track of C5 coated highlighting points Pt.3, next to the edge but out of the track, and Pt.4 within the track.

Some signs of adhesive wear can be observed in Figure 10. These signs are related to material transfer and detachment due to the localized bond between surfaces in contact, while the hard metallic specimens and asperities, during relative motion, were submitted to a friction pression. Consequently,

Table 6. EDS semi-quantitative analysis of points within, on the edge, and out of the worn track, of coated AISI 1045 samples, illustrated in Figure 10.

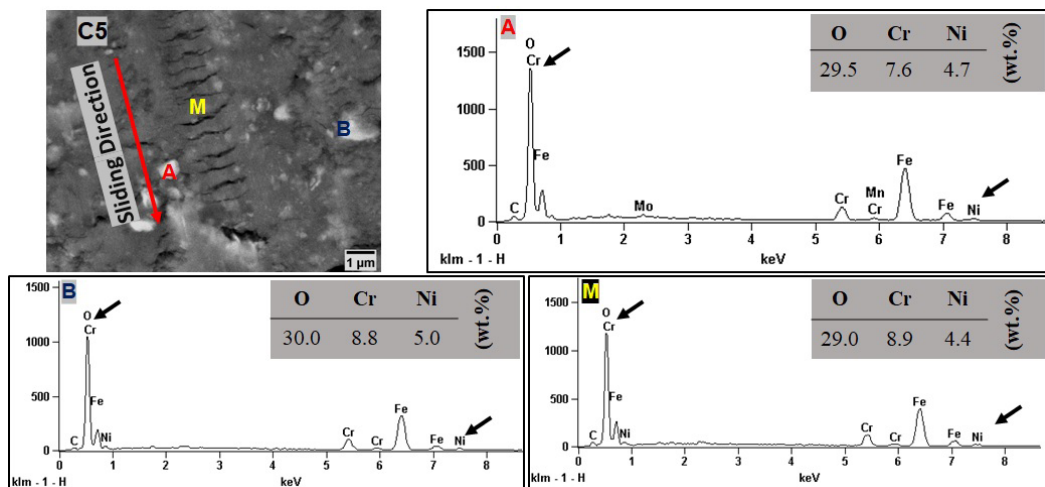| Points	Chemical composition (wt.%)							
	C	O	Al	Mn	Mo	Fe	Cr	Ni
Pt.1	1.2	11.6	0.0	1.4	1.6	61.9	14.4	7.87
Pt.2	12.0	25.8	0.49	1.1	0.0	54.3	5.7	0.0
Pt.3	0.0	0.0	0.0	2.4	0.0	71.2	16.9	9.5
Pt.4	1.7	33.4	0.0	0.0	0.0	55.3	9.6	0.0

Figure 9. SEM image within the worn wear and EDS analysis of regions M, A, and B in details.
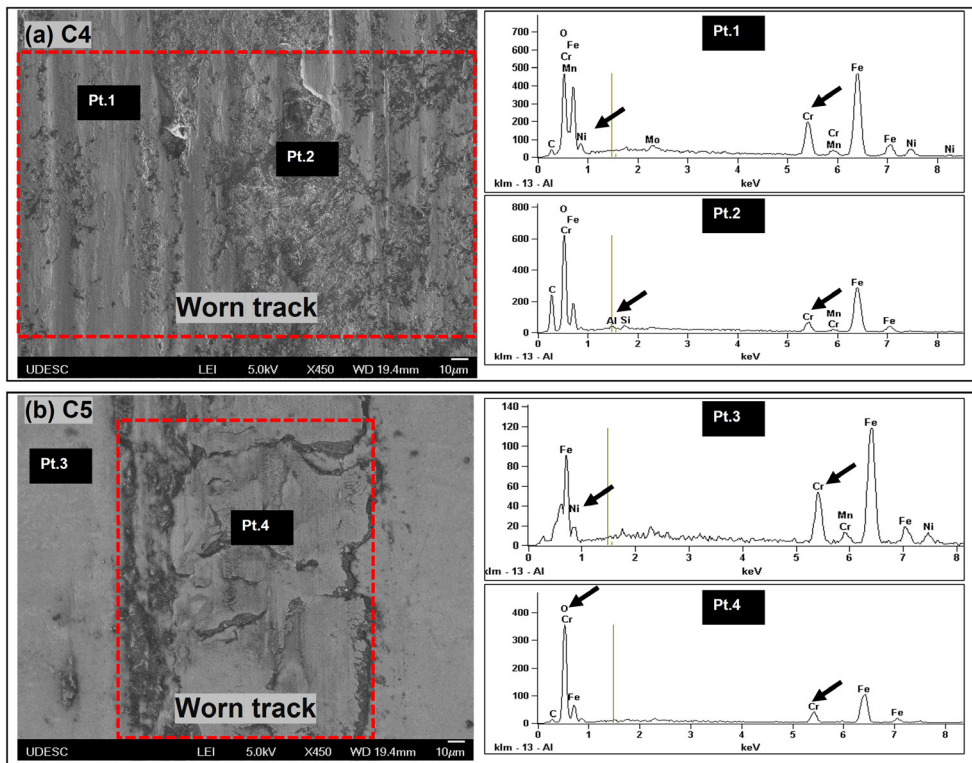
Figure 10. SEM images of the wear tracks of coated AISI 1045 (a) C4, (b) C5. EDS in regions highlighted Pt.1, Pt.2, Pt.3, and Pt.4.

the adhered junctions are sheared. Al and O can represent signs of adhesion from material of the Alumina (Al_2O_3) counter-body on the track[22-26]. Table 6 shows chemical elements' semi-quantitative values detected in points Pt.1 until Pt.4.

As shown in Table 6, Cr detection can confirm the presence of the film adhered in the worn track. Ni was also detected, although in a lower quantity than Cr. For point Pt.1, Cr was quantified at around 14 wt.% and Ni was quantified at around 8 wt.%. In contrast, in point Pt.2, Cr was quantified at around 6 wt.%, Ni was not detected, and Al was detected and quantified at around 0.5 wt.%. For point Pt.3, Cr was quantified around 17 wt.% and Ni was quantified at around 9 wt.%. In contrast, in point Pt.4, only Cr was quantified at around 10 wt.%, Ni and Al were not quantified.

Therefore, C4 configuration, presented film adhered on material despite wear, on the other hand, oxidative wear predominates within the worn track. The presence of Al on the track evidence material transfer from the counter-body to the specimen indicating signs of adhesive wear. Despite its lower probability to happen compared to oxidative wear, when materials are transferred it suggests an adhesive wear mechanism occurred. Other studies[23,28,30-32] also describe the oxide layer compacted in the center of the worn track due to the particles of the thin film transferred, which were removed from the counter-body (Al_2O_3) during the wear test, resulting in oxidation, and causing fragments, consequently a higher possibility to occur redeposition on the wear track.

On the other hand, the adhesive wear cannot be confirmed to C5 configuration, but signs of oxidative wear could be observed inside the track. It presented less material

removal combined to a thinner track width, resulting in a higher wear resistance comparing to C4 configuration, and probably better than other similar configurations (C1 to C3), and with a similar resistance compared to C6 (similar crystalline structure of C5). It can be explained by the higher content of Cr detected on the track compared to the other conditions, which indicates that the film remained adhered to the substrate on the track after the wear test.

ASS films present good adherence[2,3,11,13-15,21,27]. Nonetheless, the adhesion of ASS films coated samples reported in studies[21,27] has been considered susceptible to crack and delamination due to ductility droop when exposed to contact loads. According to Garzón et al.[27] mainly when the film is produced by a sputtering system in a non-inert flux atmosphere and without substrate heating there is a susceptibility to crack formation after indentation tests (they applied the VDI 3198). Other studies pointed lower wear damage in samples coated by magnetron sputtering with the substrate heating[3,21,27].

Therefore, it is observed that the crack formation is reduced, and the wear resistance is increased when the ASS film is deposited with substrate heating, produced in inert magnetron sputtering which results in a mixture of ferrite and austenitic phases formed. Regarding the results shown, we can consider C5 and C6 conditions with better tribological performances comparing to the other conditions of this study.

3.3. Electrochemical corrosion test

Before the electrochemical exposure test, the Open Circuit Potential (OCP) test was carried out to stabilize the

materials system in the corrosive solution of NaCl 3.5%, for 3 hours. The OCP cycle was performed to AISI 1045 coated with ASS film representing all the coated conditions and to uncoated AISI 1045. As observed in Figure 11.

Figure 11 shows that the OCP values of the uncoated AISI 1045 were more negative than the OCP values of the coated samples. The corrosion potential expected to indicate an improvement in the corrosion resistance property of the material tends to be more positive, in this case, the OCP curve shows an improvement trend in the corrosion resistance of the coated material. These more positive values can be explained by a reduction of the electrochemical activity on the sample surface, then resulting sign of protective film known as passive layer. This passive layer is generally attributed to the presence of chromium oxide (Cr_2O_3). Considering the uncoated AISI 1045 substrate, the E_{corr} values tend to be more negative, because in this case the surface is subjected to a higher corrosion, due to the absence of alloying elements that are responsible to form the passive layer[33,34].

At the end of the OCP test, the potentiodynamic polarization test was automatically started[19]. The results of the potentiodynamic polarization test can be seen in Figure 12.

Figure 12 shows the corrosion behavior of R1, R2, and R3 coatings, representing AISI 1045 coated with ASS film. A tendency to provide a corrosion resistance improvement in relation to AISI 1045 bare material is observed, manly to R2 and R3 conditions. The sample R1 show E_{corr} more negative, can be due the crystalline structure BCC, similar to substrate, which differ than other coated samples. Table 7 shows the results of some corrosion parameters extracted from the corrosion potentiodynamic polarization curves by E log | fit extrapolated[33,34].

Through the results in Table 7, it can be suggested that the materials which present better corrosion resistance, in corrosive environments or processes, have the highest corrosion potential (E_{corr}) results, thus, showing more positive E_{corr}, lower corrosion rates (CR) and lower corrent density (I_{corr}).

The coating corrosion resistance behavior depends on the corrosion solution and coating conditions. Zhao at al[35] evaluated the corrosion resistance of 316L coated samples produced by spray technique in two different solutions and the samples were more corroded in sulfuric acid than in citric acid. The electrolyte solution (3.5 wt% NaCl) is very severe for steels, mainly carbon steel samples, coated and uncoated, and this results in general corrosion without pitting points, impairing the calculation of polarization resistance. The coated samples tendency to provide a corrosion resistance

improvement in relation to AISI 1045 bare material is suggested due to the formation of a passivation film in anodic regions. In this case, R2 and R3 coatings presented better performance than uncoated AISI 1045. R2 and R3 coating samples resulted in lowest I_{corr} and CR compared to the AISI 1045 raw material. R1 sample had unexpected results[33-37].

According to Yoo et al.[2] the corrosion resistance of carbon steel coated with AISI 304 films is better than carbon
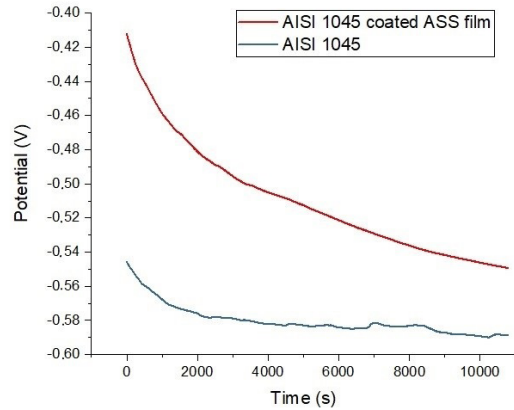

Figure 11. OCP curves of AISI 316 stainless steel (ASS) coating on the AISI 1045 material compared to the uncoated AISI 1045.
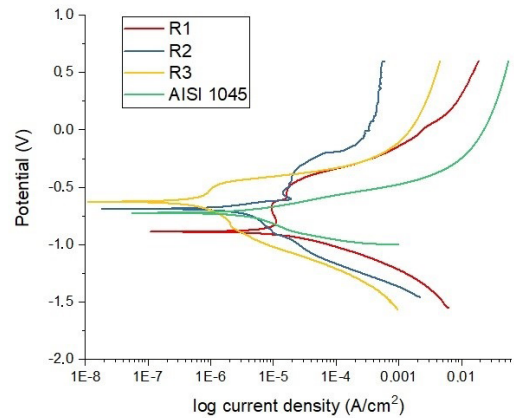

Figure 12. Potentiodynamic polarization curve of coated samples compared to uncoated AISI 1045. Start at -1 V end at +0.6 V.

Table 7. Electrochemical parameters calculated through potentiodynamic polarization curves.

Samples	Corrosion Potential E_{corr} (mV)	Current intensity I_{corr} (A/cm²)	Corrosion rate CR (mm/a)
R1*	-886.5	8.8X10⁻⁶	4.0
R2**	-687.5	0.38 X10⁻⁶	0.17
R3***	-625.0	0.53 X10⁻⁶	0.24
AISI 1045	-723.0	3.2 X10⁻⁶	1.5

*Coating **R1** was considered similar to C1 - C4 coatings, due to BCC crystalline structure. **Coating **R2** was considered similar to C6 coating, due to BCC+FCC with FCC phase predominance. ***Coating **R3** was considered similar to C5 coating. The crystalline structure and the phase proportion were related by Schoreder[9], presented in this work in Table 3.

steel substrate. This resistance has been correlated to good adhesion between films with substrate and suggests less adhesion to R1 condition compared to R2 and R3, impairing the corrosion resistance results[2,35,36].

Thus, the coated samples presented an improvement of corrosion resistance compared to AISI 1045 raw material. And this behavior may be related to the crystalline structures and phases formed by these ASS films deposited on AISI 1045 raw material. Highlighting the crystalline structures and phases when the mixture of BCC (alpha ferrite) and FCC (gamma-austenite) phases was formed. And it tends to improve even more when the austenite (γ-iron) phase is predominant.

4. Conclusion

Based on the tribological behavior and electrochemical results of uncoated AISI 1045 and coated with ASS films, it is possible to conclude that:

TMS configuration of AISI 1045 coated with ASS: The deposition conditions that presented the best tribological results were those obtained at the highest power density (15.8×10^4 W/m^2) and at a temperature of 673K. The average results of maximum depth observed through the profiles of the wear test to C1-C4 and C5-C6 conditions were 5.6 ± 1.5 μm and 1.8 ± 0.6 μm, respectively. Considering the results here found, it can be stated that the samples which present higher wear resistance were produced by magnetron sputtering with substrate heating and coatings where BCC+FCC phase were formed. The predominant mechanisms identified for the coated samples were abrasive, oxidative, and adhesive wear.

Tribological influence of the crystalline structure: AISI 1045 coated with ASS film, in the mixed crystalline structure configuration (BCC+FCC), performed the best tribological compared to other coatings with only BCC crystalline structure. C5 coated condition presented the lowest dynamic coefficient of friction, (in stage 1, before the steady state), and the C6 coated condition presented the lowest COF of all the samples studied. C5 and C6 presented the lowest wear rates, representing maximum depth/thickness ratios between 2 to 6 times lowest than BCC configurations.

Corrosion resistance tendency of the crystalline structure: Regarding OCP and potentiodynamic polarization test, the coated samples which presented a mixture of crystalline structures BCC (α-Ferrite) and FCC (γ-iron), mainly when austenite-γ phase was predominant, resulted in better resistance corrosion comparing to uncoated AISI 1045.

5. Acknowledgments

6. References

1. Bateni MR, Szpunar JA, Wang X, Li DY. Wear and corrosion wear of medium carbon steel and 304 stainless steel. Wear. 2006;260(1-2):116-22.

2. Yoo JH, Ahn SH, Kim JG, Lee SY. Influence of target power density and substrate bias voltage on the electrochemical properties of type 304 SS films prepared by unbalanced magnetron sputtering. Surf Coat Tech. 2002;157(1):47-54.

3. España Peña CL, Recco AA, Olaya JJ. A microstructural and wear resistance study of stainless steel-ag coatings produced through magnetron sputtering. Coatings. 2018;8(11):381.

4. Abegunde OO, Akinlabi ET, Oladijo OP, Akinlabi S, Ude AU. Overview of thin film deposition techniques. AIMS Mater Sci. 2019;6(2):174-99.

5. Fontana LC. Estudo da deposição de filmes de Ti e TiN e desenvolvimento do sistema modificado triodo-magnetron-sputtering [thesis]. Florianópolis: Universidade Federal de Santa Catarina; 1997.

6. Fontana LC, Muzart JL. Characteristics of triode magnetron sputtering: the morphology of deposited titanium films. Surf Coat Tech. 1998;107(1):24-30.

7. Fontana LC, Muzart JL. Triode magnetron sputtering TiN film deposition. Surf Coat Tech. 1999;114(1):7-12.

8. Recco AA, Muzart JR, Fontana LC. Deposição de filmes de TiN e TiO por Triodo-magnetrun sputtering. In: Congresso Brasileiro de Engenharia e Ciência dos Materiais (CBECiMat); 2002; Natal. Anais. São Paulo: ABCeram, ABM, ABPol; 2002. p. 1333-7.

9. Schroeder MV. Obtenção e caracterização de filmes de aço inoxidável 316 obtidos por pulverização catódica [dissertation]. Joinville: Universidade do Estado de Santa Catarina; 2017.

10. Schroeder MV, Recco AA. Influência da densidade de potência e da porcentagem de N$_2$ na atmosfera de deposição na dureza e no módulo de Young em filmes de aço inoxidável AISI 316 depositados por pulverização catódica. Materia. 2019;24(1):e12338.

11. Schroeder MV, Recco AA, Garzón CM. Tailoring the phase fractions by tuning the pulse frequency in stainless steel films obtained from an 316L target by pulsed-DC magnetron sputtering. Mater Lett. 2018;230:20-3.

12. Liu L, Li Y, Wang F. Influence of grain size on the corrosion behavior of a Ni-based superalloy nanocrystalline coating in NaCl acidic solution. Electrochim Acta. 2008;53(5):2453-62.

13. Seelam UM, Suryanarayana C. Metallography of sputter-deposited SS304+ Al coatings. Metallogr Microstruct Anal. 2013;2(5):287-98.

14. Garzón CM, Vergara GA, Recco AA. The effects of constrained atomic partitioning among FCC and BCC phases on nitrogen absorption in films that are reactively magnetron-sputtered from an 316L target. Mater Lett. 2017;206:34-8.

15. Garzón CM, Recco AA. Numerical simulation on phase stability between austenite and ferrite in steel films sputter-deposited from austenitic stainless-steel targets. Surf Coat Tech. 2018;353:84-92.

16. Sedlaček M, Podgornik B, Vižintin J. Correlation between standard roughness parameters skewness and kurtosis and tribological behaviour of contact surfaces. Tribol Int. 2012;48:102-12.

17. Blau PJ. Friction science and technology: from concepts to applications. Boca Raton: CRC Press; 2008.

18. Archard JF, Hirst W. The wear of metals under unlubricated conditions. Proc R Soc Lond A Math Phys Sci. 1956;236(1206):397-410.

19. Gamry Instruments. Framework operator's manual corrosion measurement system 100. Warminster; 2022.

20. Stachowiak GW, Batchelor AW. Engineering tribology. Oxford: Butterworth-Heinemann; 2013.

21. España Peña CL, Recco AA, Olaya Flórez JJ. Tribological evaluation of ferritic-austenitic stainless steel coatings with different percentages of silver. Mater Res. 2022;25:e20220078.

22. Godfrey D. Friction oscillations with a pin-on-disc tribometer. Tribol Int. 1995;28(2):119-26.

23. Zappelino BF, Almeida ED, Krelling AP, Costa CE, Fontana LC, Milan JC. Tribological behavior of duplex-coating on Vanadis 10 cold work tool steel. Wear. 2020;442:203133.

24. Holmberg K, Matthews A, Ronkainen H. Coatings tribology: contact mechanisms and surface design. Tribol Int. 1998;31(1-3):107-20.

25. Menezes PL, Nosonovsky M, Ingole SP, Kailas SV, Lovell MR, editors. Tribology for scientists and engineers. New York: Springer; 2013.

26. Holmberg K, Matthews A. Coatings tribology: properties, mechanisms, techniques and applications in surface engineering. Amsterdam: Elsevier; 2009.

27. Garzón CM, Vergara GA, Recco AA. The effect of nitrogen flow rate on the loadbearing capacity from nano-to macro-hardness of austenitic stainless steels magnetron sputtering-coated with stainless steel films. Mater Res. 2020;23(3):e20190453.

28. dos Santos de Almeida EA, Milan JC, da Costa CE, Binder C, de Mello JD, Costa HL. Combined use of surface texturing, plasma nitriding and DLC coating on tool steel. Coatings. 2021;11(2):201.

29. Rovani AC, Breganon R, de Souza GS, Brunatto SF, Pintaúde G. Scratch resistance of low-temperature plasma nitrided and carburized martensitic stainless steel. Wear. 2017;376:70-6.

30. Zum Gahr KH. Microstructure and wear of materials. Amsterdam: Elsevier; 1987.

31. Almeida ED, Milan JC, Costa HL, Krelling AP, Costa CE. Sliding wear of borided sintered AISI M2 steel coated with AlTiN/CrN multilayer. Wear. 2018;410:11-24.

32. Hutchings I, Shipway P. Tribology: friction and wear of engineering materials. Oxford: Butterworth-Heinemann; 2017.

33. Wong LL, King KJ, Martin SI, Rebak RB. Methods of calculation of resistance to polarization (corrosion rate) using ASTM G 59. Livermore: Lawrence Livermore National Laboratory; 2006.

34. Panossian Z, Cardoso JL. Interpretação de curvas de polarização. In: INTERCORR ABRACO; 2014; Fortaleza, CE. Anais. Rio de Janeiro: Associação Brasileira de Corrosão; 2014.

35. Zhao L, Lugscheider E. Influence of the spraying processes on the properties of 316L stainless steel coatings. Surf Coat Tech. 2003;162(1):6-10.

36. Zhao Y, Liu W, Fan Y, Zhang T, Dong B, Chen L, et al. Influence of microstructure on the corrosion behavior of super 13Cr martensitic stainless steel under heat treatment. Mater Charact. 2021;175:111066.

37. Habeeb HJ, Luaibi HM, Dakhil RM, Kadhum AA, Al-Amiery AA, Gaaz TS. Development of new corrosion inhibitor tested on mild steel supported by electrochemical study. Results Phys. 2018;8:1260-7.